Combined Effect of Organic Phosphate Sodium and Nanoclay on the Mechanical Properties and Crystallization Behavior of Isotactic Polypropylene

Shicheng Zhao, Zhong Xin, Jing Zhang, Ting Han

State-Key Laboratory of Chemical Engineering, Department of Product Engineering, East China University of Science and Technology, Shanghai 200237, People's Republic of China

Received 29 November 2010; accepted 19 March 2011
DOI 10.1002/app.34527
Published online 28 July 2011 in Wiley Online Library (wileyonlinelibrary.com).

ABSTRACT: Combined effect of α-nucleating agent (NA) sodium 2,2′-methylene-bis(4,6-di-*tert*-butylphenyl) phosphate (NA11) and nanoclay (NC) on the mechanical properties and crystallization behavior of isotactic polypropylene (iPP) was investigated by mechanical testing, wide-angle X-ray scattering (WAXD), differential scanning calorimetry (DSC), polarized optical microscopy (POM), and scanning electron microscopy (SEM). The mechanical testing results indicated that the separate addition of NA11 and NC only increased the stiffness of iPP while the combined addition of NA11, NC, and maleic anhydride grafted polypropylene (PP-*g*-MA) simultaneously improved stiffness and toughness of iPP. Compared to pure iPP, the tensile strength, the flexural modulus, and impact strength of iPP composites increased 9.7, 38.6, and 42.9%, respectively. The result indicated good synergistic effects of NC, NA11, and PP-*g*-MA in improving iPP mechanical properties. WAXD patterns revealed NA11, and NC only induced the α-crystals of iPP. SEM micrograph showed that the PP-*g*-MA could effectively improve the dispersing of NC in iPP. Finally, the nonisothermal crystallization kinetics of neat iPP and PP nanocomposites was described by Caze method. The result indicated that the addition of NA overcame the shortcoming of low crystallization rate of NC nanocomposites and maintained the excellent mechanical properties, which is another highlight of the combined addition of NAs and nanoclay. Meanwhile, the result showed that nuclei formation and spherulite growth of iPP were affected by the presence of NA and nanoclay. © 2011 Wiley Periodicals, Inc. J Appl Polym Sci 123: 617–626, 2012

Key words: mechanical properties; crystallization behavior; polypropylene; nucleating agent; nanoclay

INTRODUCTION

Isotactic polypropylene (iPP) is one of the most important commercial polymers due to its relatively low cost, low density, high-heat distortion temperature (HDT), and good mechanical properties.[1] However, the need for materials with superior mechanical, thermal, and processing properties cannot be overemphasized. To improve polypropylene's competitiveness in engineering resin application, it is desirable and important to increase dimensional stability, HDT, stiffness, strength and impact resistance, and processability.

In industry, α-nucleating agent (NA) is widely used to improve the performance of iPP.[2–9] The NAs can provide higher crystallization temperature, create a large number of smaller spherulites, and improve the optical and mechanical properties of iPP. Small spherulites of iPP may improve its flexural modulus and rigidity. The size reduction of spherulites positively affects the optical properties, reducing haze, and hence improving clarity.[5] The higher crystallization temperature cannot only significantly reduce the cycle's time but also raise the output of product.[6–8] At present, the widely used NAs are sorbitol derivatives and organic phosphate salts. Sorbitol-based nucleators could provide significant improvement to the crystallization rate and clarity of iPP.[4] Metal salts of substituted aromatic heterocyclic phosphate were found to be very promising nucleators for PP matrices.[9] In particular, sodium 2,2′-methylene-bis(4,6-di-*t*-butylphenylene)phosphate (NA11) widely used in the processing of iPP is a powerful NA, which can effectively improve the strength and modulus of iPP.

Another commonly used method improving the properties of iPP and reducing cost is adding the filler, especially nanoparticle.[10–12] Polypropylene-layered silicate nanocomposites, which are the subject of the present contribution, are prepared by

Correspondence to: Z. Xin (xzh@ecust.edu.cn).
Contract grant sponsor: Program of Shanghai Subject Chief Scientist; contract grant number: 10XD1401500.
Contract grant sponsor: National Natural Science Foundation of China; contract grant number: 20876042.
Contract grant sponsor: "the Fundamental Research Funds for the Central Universities".

incorporating finely dispersed layered silicate materials in PP matrix. The resulting polymer-layered silicates hybrids possess unique properties—typically not shared by their more conventional microscopic counterparts—which are attributed to their nanometer size features and the extraordinarily high surface area of the dispersed clay.[13,14] In fact, it is well established that dramatic improvements in physical properties, such as tensile strength and modulus, HDT, and gas permeability, can be achieved by adding just a small fraction of clay to a polymer matrix, without impairing the optical homogeneity of the material. The most notable effect is the unexpected properties obtained from the addition of stiff filler to a polymer matrix, for example, the often reported retention (or even improvement) of the impact strength.

However, nanoclay is not easily dispersed in PP due to their preferred face-to-face stacking in agglomerated tactoids. Dispersion of the tactoids into discrete monolayers is further hindered by the intrinsic incompatibility of hydrophilic layered silicates and hydrophobic polypropylene matrix. To improve compatibility between the clay and nonpolar polymers, the hydrophilic clay surface can be modified by ion-exchange reaction with a quaternary alkylammonium salts to reduce its polarity, and then an organophilic clay is obtained.[15,16] Additionally, the compatibilizer is used to improve the compatibility between the organically modified clay and the polymeric matrix.[16–18] Maleic anhydride grafted polypropylene (PP-*g*-MA) is the most commonly used compatibilizer.[16,17] It is believed that the polar character of the anhydride has an affinity for the clay materials.

As the single application of NA and nanoclay can significantly improve the properties of iPP, therefore, it arouses great interest to investigate the combined effects of NA and nanoclay on the mechanical properties and crystallization behavior of iPP. So far, there is little report on this investigation. In this work, NA11 was chosen, because it can significantly increase the tensile strength and flexural modulus of iPP. NA11 and NC were added into iPP matrix, and PP-*g*-MA was used as the compatibilizer to prepare iPP–clay nanocomposites. Their combined effects on the mechanical properties and crystallization behavior of iPP nanocomposites were investigated.

EXPERIMENTAL

Materials

The iPP sample (trade name T30S) was provided by Jiujiang Petroleum Chemical Co., China, with a melt flow rate of 2.9 g/10 min (230°C/2.16 kg), M_w = 24.4 × 10^4 g mol^{-1}, and M_w/M_n = 4.05. A natural montmorillonite clay surface-modified with dimethyl dialkyl ammonium (Nanomer I.44P, Nanocor) was used as the reinforcement filler. A commercially available NA of sodium 2,2′-methylene-bis(4,6-di-*tert*-butylphenyl) phosphate (Irgastab NA-11, Ciba Specialty Chemicals, Switzerland) was selected. PP-*g*-MA (Nanjing Deba Chemical Co.) was used. The particle shapes of NA11 and NC are showed in Figure 1. The grafting percentage of MA was determined to be 0.85%, and the melt flow index was 35 g/10 min at 230°C/2.16 kg. The nanocomposites were prepared by mixing the appropriate amounts in a twin screw extruder (screw speed, 100 rpm) followed by injection molding of tensile, flexural, and Izod impact bars.

TABLE I
The Content of the Nucleating Agent and Nanoclay in the Nanocomposites

Sample	Nucleating agent (wt %)	Nanoclay (wt %)	PP-*g*-MA (wt %)
PP1	0	0	0
PP2	0	4	0
PP3	0	0	5
PP4	0	4	5
PP5	0.1	0	0
PP6	0.1	4	0
PP7	0.1	4	5

Sample preparation

The NA (0.1 wt %), nanoclay (typically 4 wt % loading), and PP-*g*-MA (5 wt %) were added into the iPP powders according to Table I. The compound was dry-blended by high-speed mixer for 5 min. Then, the mixture was extruded by a twin-screw extruder (SJSH-30, Nanjing Rubber and Plastics Machinery Plant Co.) through a strand die and pelletized. The pellets were molded into standard test specimens by an injection-molding machine (CJ-80E, Guangdong Zhende Plastics Machinery Plant Co.). The concentrations of the NA, nanoclay, and PP-*g*-MA were listed in Table I.

Mechanical properties

The mechanical properties were measured according to ASTM test methods, such as D-638 for the tensile strength and D-790 for the flexural modulus, using a universal testing machine (Shanghai D and G Measure Instrument Co.). The Izod impact strength was tested on the basis of D-256, using an impact tester (Chengde Precision Tester Co.). The reported values of the mechanical properties were averaged at five independent measurements.

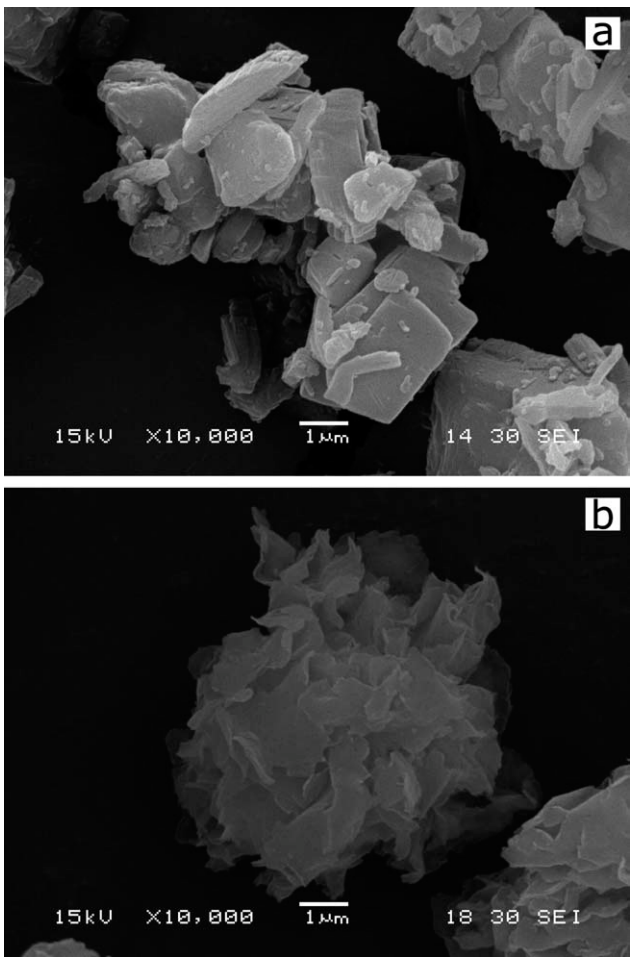

Figure 1 SEM micrographs of α-nucleating agent NA11 (a) and nonoclay (b).

Wide-angle X-ray scattering

Wide-angle X-ray scattering (WAXD) sample was cut from the flexural bar, which was shown in Figure 2.

WAXD patterns were recorded in transmission with a Rigaku D/max-2550VB/PC apparatus. The wavelength of Cu Kα was $\lambda = 1.54$ E, and spectra were recorded in the 2θ range of 10°–30° (6°/min). The content of the β-crystal modification was determined according to standard procedures described in the literature,[19] using the relation of Eq. (1):

$$k_\beta = \frac{H_\beta(300)}{H_\beta(300) + H_\alpha(110) + H_\alpha(040) + H_\alpha(130)} \quad (1)$$

where k_β denotes the relative content of β-crystal form (WAXD), H_α (110), H_α (040), and H_α (130) are the intensities of the highest peaks of α-form attributed to the (110), (040), and (130) planes of monoclinic cell, respectively, while H_β (110) is the intensity of the highest (110) diffraction peak of the trigonal β-form. $H_\Omega(hkl)$ denotes the intensity of the respective (hkl) peak belonging to phase Ω (α or β; always with respect to the amorphous halo).

Differential scanning calorimetry

Differential scanning calorimetry (DSC; Diamond, Perkin–Elmer) was carried out to measure the crystallization peak temperature and analyze the nonisothermal crystallization kinetics. The temperature was calibrated before the measurements by using indium as a standard medium.

The crystallization peak temperature (T_{cp}) was determined from the crystallization curves. Measurements were performed with the samples of 3–5 mg at a standard heating and cooling rate of 10°C/min under nitrogen starting from 50 to 200°C, and the samples were held at 200°C for 5 min to erase the thermal and mechanical history.

Nonisothermal crystallization experiments were carried out by cooling samples from 200 to 50°C by using different cooling rates. The exotherms were recorded at the cooling rates of 2.5, 5, 10, 20, and 40°C/min, respectively.

Polarized optical microscopy

The morphology studies of pure iPP and nucleated iPP were performed with the aid of an Olympus BX51 (Japan) polarized optical microscopy (POM) attached with a DP70 digital camera and a THMS600 hot-stage. The extruded samples were placed between two microscopy slides, melted, pressed at 200°C for 5 min to erase any trace of crystal, and then crystallized at the cooling rate of 10°C/min. The photographs were automatically taken at 50°C.

Theory of nonisothermal crystallization

The Avrami equation [Eq. (2)][20,21] is widely used to describe the polymer isothermal crystallization.

$$X_t = 1 - \exp(-Z(T)t^n) \quad (2)$$

where X_t is the relative crystallinity at t, n is a constant whose value depends on the characteristics of nucleation and the form of crystal growth, and $Z(T)$ is a constant containing the nucleation and growth parameters.

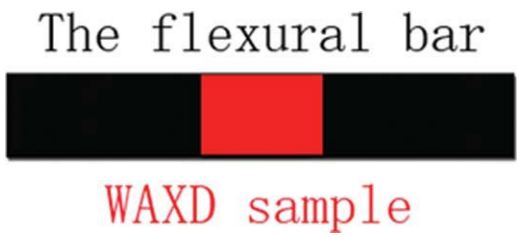

Figure 2 WXRD samples cutting from the flexural bar. [Color figure can be viewed in the online issue, which is available at wileyonlinelibrary.com.]

The Avrami equation has been extended by Ozawa[22] to study the nonisothermal experiment. The general form of Ozawa theory is written as follows:

$$X_v(T) = 1 - \exp(-K_T/\phi^m) \quad (3)$$

where K_T is the cooling crystallization function, φ is the cooling rate, and m is the Ozawa exponent that depends on the dimension of the crystal growth. But, there is a main hypothesis in Ozawa method that m is independent of temperature, and only a limited number of X_v data are available for the foregoing analysis, as the onset of crystallization varies considerably with the cooling rate.

Caze et al.[23] put forward a new method to modify Ozawa equation. They have assumed an exponential increase of K_T with T upon cooling. On this basis, the temperature at the peak and the two inflection points of the exotherm with skew Gaussian shape are linearly related to ln ϕ to estimate the exponent n.

On the basis of the findings on the crystallization behavior of poly(ethylene terephthalate) and PP, Kim et al.[24] proposed:

$$\ln K_T = a(T - T_1) \quad (4)$$

where a and T_1 are empirical constants. If the extreme point of the pertinent $\partial X_v(T)/\partial T$ curve occurs at $T = T_q$ (crystallization peak temperature), that is, $(\partial^2 X_v(T)/\partial T^2)T_q = 0$, we have Eq. (5):

$$K_T(T_q) = \phi^n \quad (5)$$

Combining eqs. (3)–(5) yields Eq. (6):

$$\ln[-\ln(1 - X_v(T))] = a(T - T_q) \quad (6)$$

Hence, a linear plot of $\ln[-\ln(1 - X_v(T))]$ against T would result in the constant a and the product $-aT_q$ from the gradient and intercept, respectively. At $T = T_q$ obtained from the foregoing algorithm, eqs. (4) and (5) lead to Eq. (7):

$$T_q = n \ln \phi/a + T_1 \quad (7)$$

As such, parameter n can be obtained from the linear plot of T_q against ln φ/a in accordance with Eq. (7).

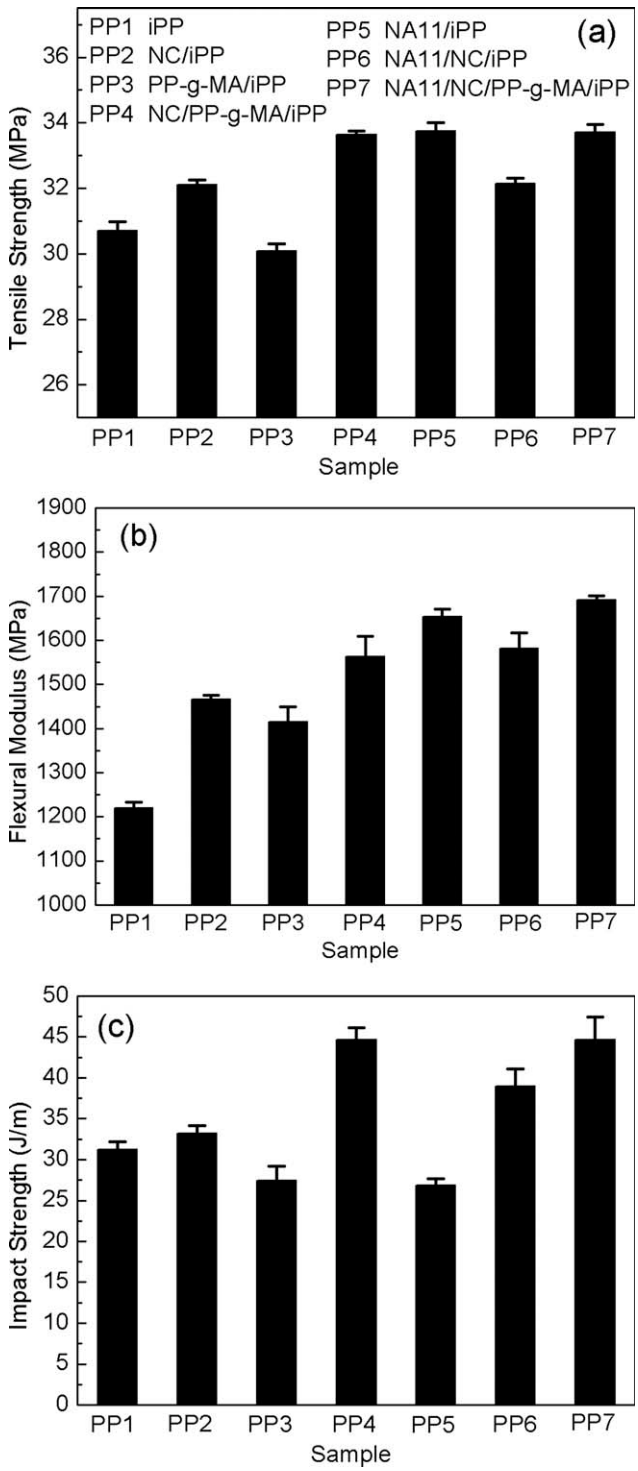

Figure 3 The effect of NA11 and nanoclay on the mechanical properties of iPP; (a) tensile strength, (b) flexural modulus, and (c) impact strength.

RESULTS AND DISCUSSION

Mechanical properties

From the viewpoint of industrial application, it is necessary to investigate the effect of NA and nanoclay on mechanical properties. The effect of the NA NA11 and nanoclay on mechanical properties of iPP is shown in Figure 3. Clearly, the single addition of NA11 and NC obviously increases the tensile strength and flexural modulus of iPP, however, slightly changes the impact strength of iPP. When PP-*g*-MA was added to NC/iPP system, the improvement effect on the impact strength was

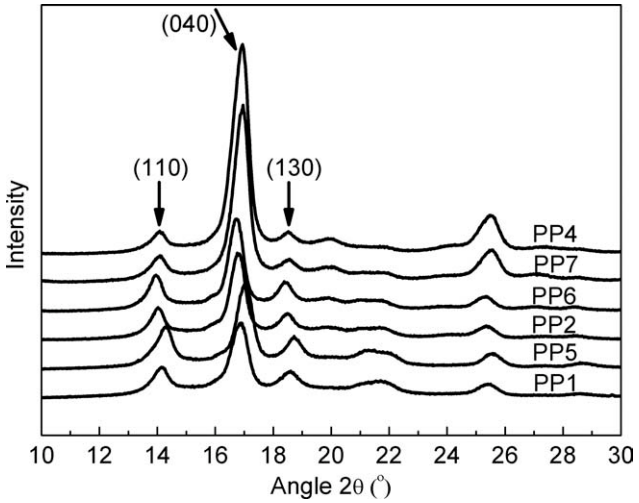

Figure 4 WAXD patterns of neat iPP and PP nanocomposites samples.

more obvious. The result indicated that the PP-*g*-MA significantly improves the compatibility of NC and iPP matrix. When the combined addition of NA11, NC, and PP-*g*-MA into iPP, stiffness, and toughness of iPP was simultaneously increased compared to NC/iPP (PP2), NA11/iPP (PP5), or NA11/NC/iPP (PP6). The system (PP7) showed good comprehensive mechanical properties comparing with separate adding NC or NA11 in iPP. Compared to pure iPP, the tensile strength, the flexural modulus, and impact strength of PP7 increased 9.7, 38.6, and 42.9%, respectively. The result indicated good synergistic effects of NC, NA11, and PP-*g*-MA in improving iPP mechanical properties.

Effect of the NA and nanoclay on the crystal structure and morphology of iPP

The effect of the NA NA11 and nanoclay I.44P on the crystalline morphology of iPP as evaluated by WAXD in the 2θ range of 10°–30° is presented in Figure 4. In this profile, (110) at 2θ = 14.1°, (040) at 16.9°, and (130) at 18.5° are the principal reflections of the α-crystals of iPP. They are considered as the marker peaks for α-crystals. As shown in this figure, the peak position of the crystal planes did not shift with the addition of NA11 and I.44P. This indicates that the typical pattern of α-crystalline iPP is not affected by the presence of NA NA11 and nanoclay I.44P. Some researchers ever reported that NC can induce the β-crystals of iPP.[25] But, in our study, the phenomenon was not found, which may be attributed to the effect of the content of NC on the crystals. The addition of higher amount of NC results to the weaker β nucleation effect.[25]

POM could provide the direct observation of crystal morphology of polymer. Therefore, POM was used to compare the crystal morphology of PP nanocomposites developed during nonisothermal crystallization process. The micrographs for neat iPP and nanocomposite samples crystallized at cooling rate 10°C/min were shown in Figure 5. As can be seen from Figure 5, nanoclay slightly decreases the size of iPP crystals while NA NA11 significantly decreases the size of iPP crystals. Meanwhile, it was found that the crystals size of all the samples incorporating NA11 greatly decrease compared to the sample NC/iPP. The results indicated that the NA11 plays a dominant nucleation in these compound systems. Another interesting phenomenon is that among all the systems incorporating NA11, the order of crystal size is as follows: NA11/iPP < NA11/NC/iPP < NA11/NC/PP-*g*-MA/iPP. The result showed that NC and PP-*g*-MA hinder the nucleation crystallization of iPP in the presence of NA.

The effect of compatibilizer on distribution of nanoclay in iPP matrix

The simple mixing of polymer and nanoclay does not always result in the generation of a nanocomposite, as this usually leads to dispersion of stacked sheets. This failure is due to the weak interaction between the polymer and the inorganic component. If the interaction becomes stronger, then the inorganic phase would be dispersed in the organic matrix in nanometer scale. Therefore, the hydrophilic silicate surface of clay was converted to organophilic, and PP-*g*-MA as compatibilizer was added into iPP to improve the interaction between the matrix and nanoclay.

To investigate the effect of compatibilizer (PP-*g*-MA) on the dispersion of clay layers in iPP matrix, scanning electron microscopy (SEM) was used, because the technique can provide the direct observation of the state of dispersion of clay platelets in the composites. The samples were immersed in liquid nitrogen for 10 min and then fractured. The SEM scanned fractured surfaces. SEM micrographs of iPP nanocomposites samples are shown in Figure 6. NA NA11 particles can be seen from Figure 6(b). The diameter of particles is less than 1 μm, which indicates that there is no obvious agglomeration in composites. Nanoclay I.44P obviously aggregates in the samples NC/iPP and NC/NA11/iPP from the Figure 6(c,d). With the addition of PP-*g*-MA [Fig. 6(e,f)], the aggregation is greatly improved. It is clear that the presence of PP-*g*-MA significantly improves the interaction of NC and the matrix leading to better dispersion of the clay. This may be due to strong interaction between polar groups of PP-*g*-MA molecules and the silicate layer.

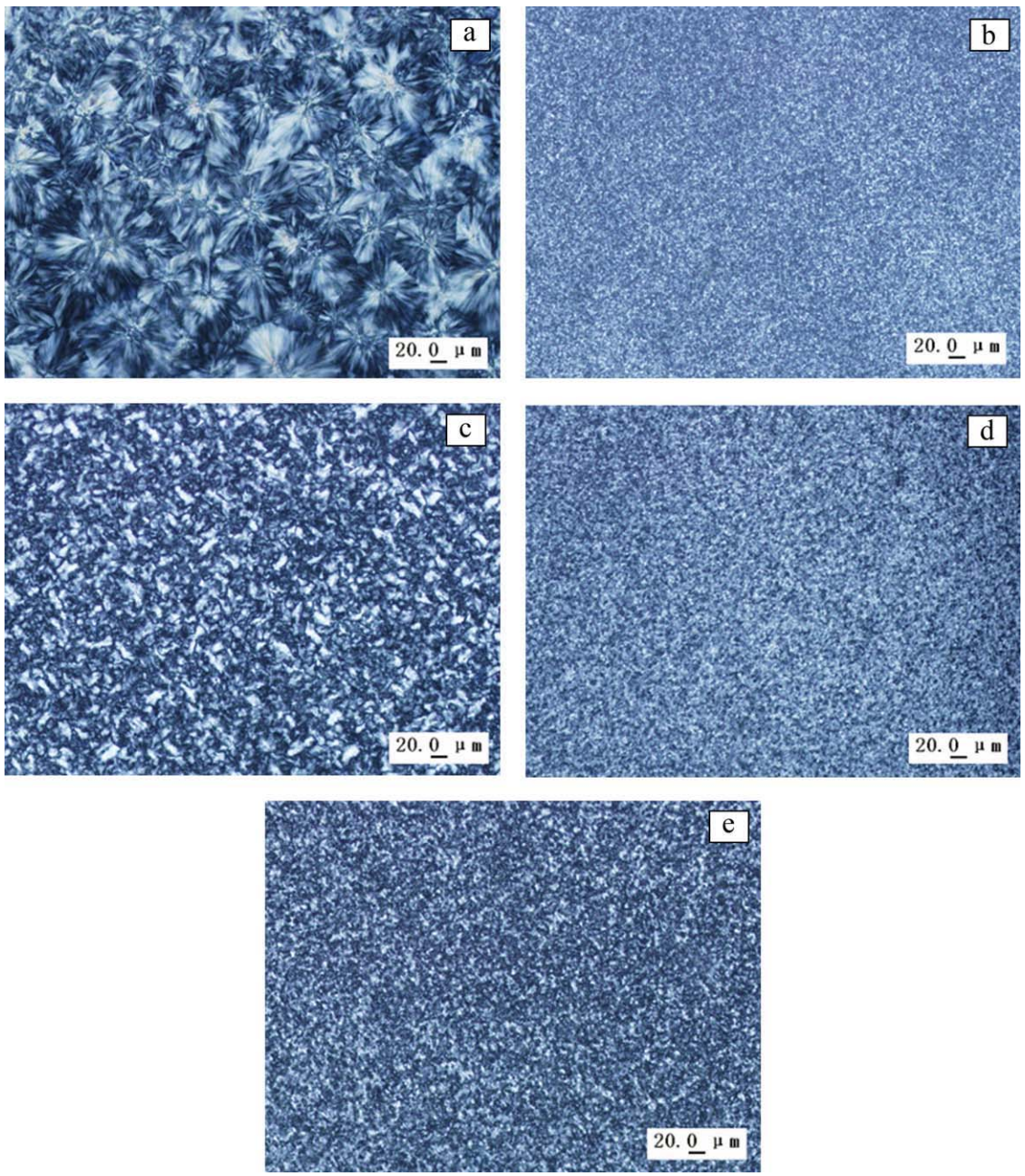

Figure 5 Polarized light microphotographs of morphology of pure iPP and PP nanocomposites; (a) iPP, (b) NA11, (c) NC, (d) NA/NC, and (e) NA/NC/PP-*g*-MA. [Color figure can be viewed in the online issue, which is available at wileyonlinelibrary.com.]

Nonisothermal crystallization kinetics

For a better understanding of the effect of NA and nanoclay on the crystallizatization behavior of iPP, DSC nonisothermal crystallization experiments were carried out. The DSC scans of neat iPP and iPP containing NA11 and NC recorded during nonisothermal cystallization of investigated samples at cooling rates from 2.5 to 40°C/min are given in Figure 7. The DSC scans of other samples are similar to that of iPP/NA11/NC. From these crystallization curves of samples, the crystallization peak temperature at different cooling rates can be obtained, and the results are plotted in Figure 8.

As shown in Figure 8, the addition of 4 wt % nanoclay into iPP matrix caused the crystallization peak temperature (T_{cp}) to slightly increase especially at higher cooling rates. The result showed weak nucleation ability of nanoclay during crystallization in quiescent condition. Compared to neat iPP, T_{cp} of iPP incorporated 5 wt % maleic anhydride-grafted iPP (PP-*g*-MA) obviously decreased. The addition of 4 wt % clay into iPP/PP-*g*-MA system caused the

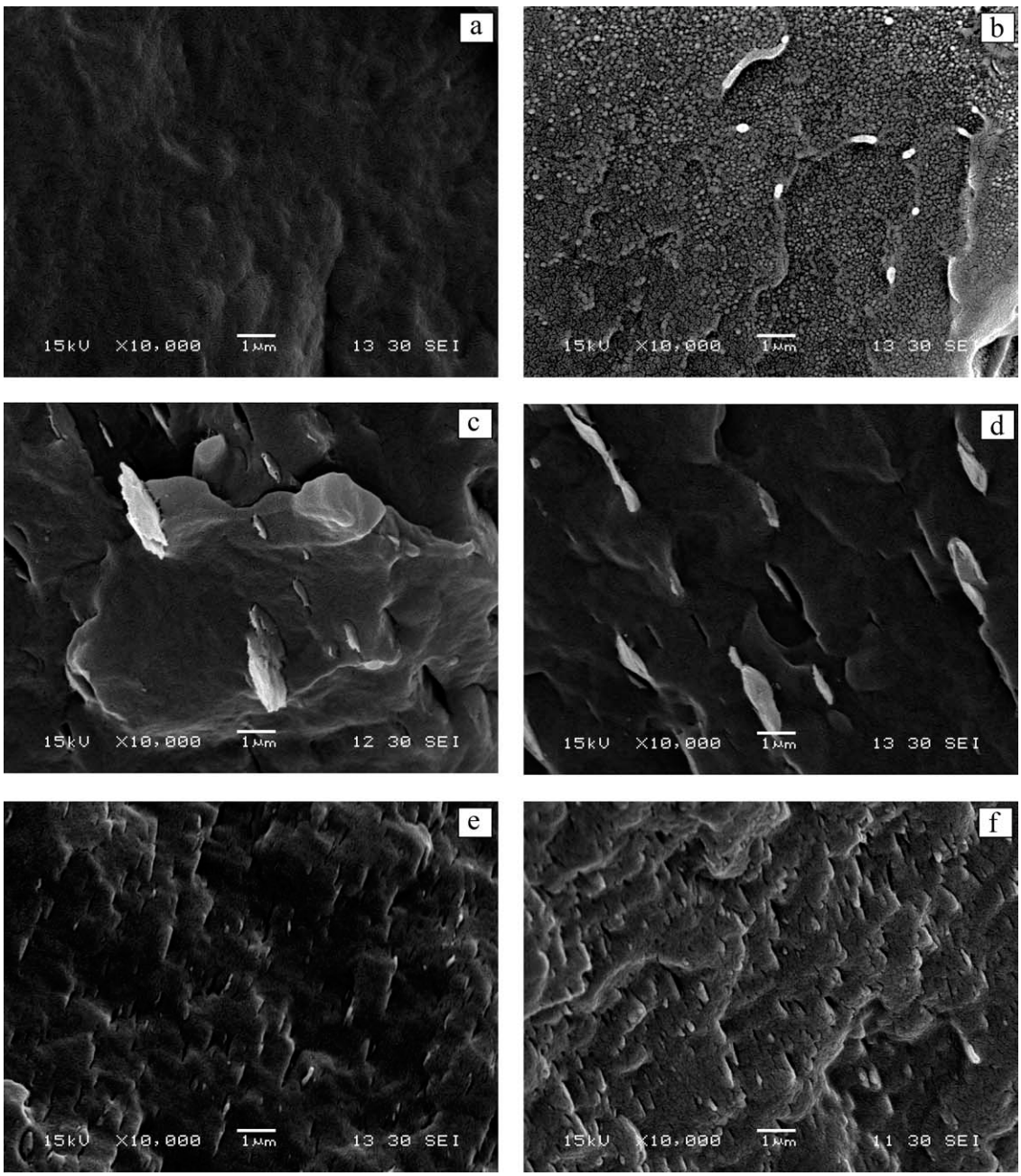

Figure 6 SEM micrograths of neat iPP and PP nanocomposites; (a) iPP, (b) NA11, (c) NC, (d) NA/NC, (e) NC/PP-*g*-MA, and (f) NA/NC/PP-*g*-MA.

crystallization peak temperature to obviously increase. The addition of PP-*g*-MA improves the dispersion of NC, which has been confirmed by the SEM micrograph. Thereby, the nucleation ability of NC is increased with the addition of PP-*g*-MA, which results in the increase of the T_{cp}. The addition of 0.1 wt % NA NA11 greatly increased the T_{cp} of iPP, which showed strong nucleation ability of NA11. In addition, it is found that the T_{cp} of the samples incorporating the NA11 is significantly increased compared to that of NC/iPP. The result indicated that the addition of NA11 into the nanocomposite could significantly reduce cycle's time and raises the output of product. The addition of NAs overcomes the shortcoming of low crystallization rate of NC nanocomposites, which is the highlight of the compounded addition of NAs and NC into iPP. Besides, it is worth to notice that the compound addition of nanoclay and NA11 decreases the T_{cp} of the system compared to NA11/iPP, which is attributed to the retardation of NC on iPP segment migration during crystal growth.[25,26] The effect of NA11 and NC on the T_{cp} is agreement with their effect on the crystals size, which is observed by POM.

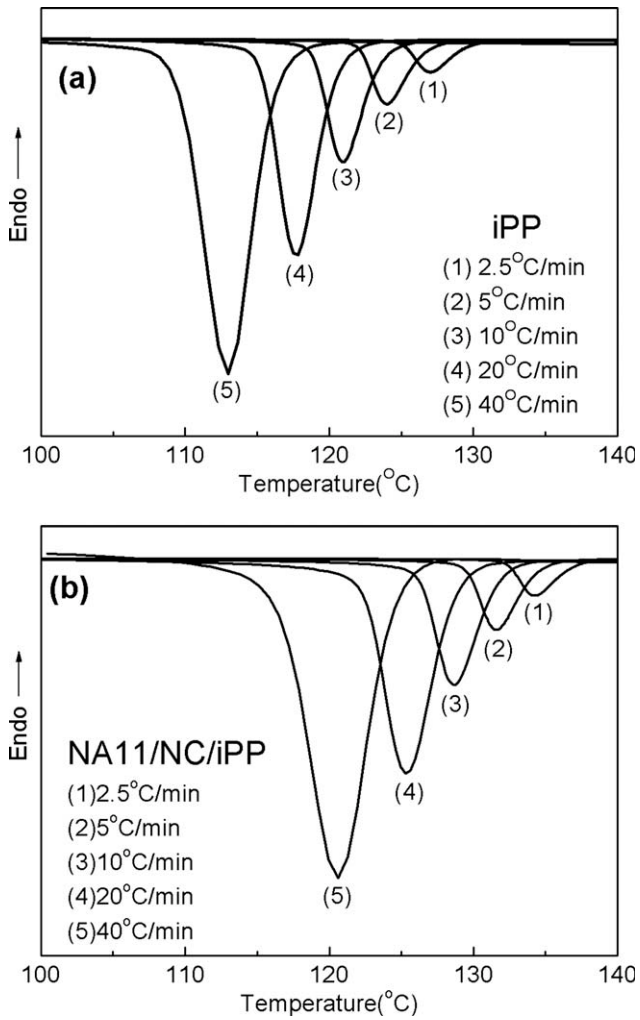

Figure 7 DSC cooling curves of (a) neat iPP and (b) NA11/NC/iPP.

By means of integrating the partial areas under the DSC endotherm, the values of the crystalline weight fraction $X_w(T)$ can be obtained, which are shown in Figure 9.

Crystallization half-time $t_{1/2}$ can be obtained from Figure 9 by the equation $t = (T_0 - T)/\varphi$ (where t is the crystallization time, T_0 is the onset crystallization temperature, T is the crystallization temperature at $X_w(T) = 50\%$, and φ is the cooling rate). The results are listed in Table II.

Now, the crystallization weight fraction $X_w(T)$ can be converted into the volume fraction $X_v(T)$ by Eq. (9)[24]:

$$X_v(T) = \frac{X_w(T)\frac{\rho_a}{\rho_c}}{1 - \left(1 - \rho_a/\rho_c\right)X_w(T)} \quad (9)$$

where ρ_a and ρ_c are the bulk densities of the polymer in the amorphous and pure α-crystalline states. For iPP, the density of the amorphous phase is $\rho_a =$ 0.852 and that of the pure α crystalline phase is $\rho_{c\alpha} = 0.936$.[27,28] Accordingly, plots of $\ln[-\ln(1 - X_v(T))]$ versus T can be obtained (Fig. 10) and showed a good linear relationship in the initial crystallization

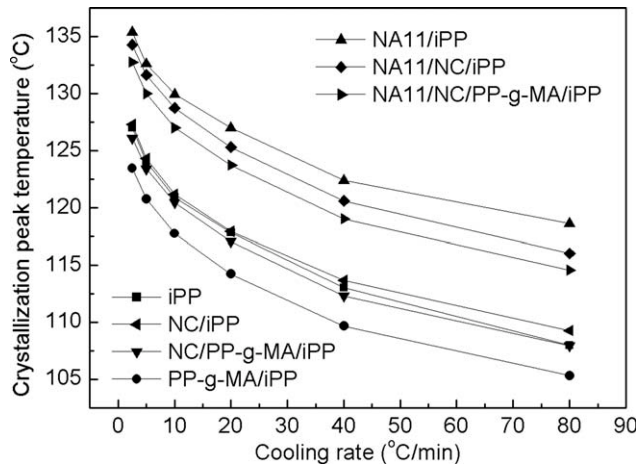

Figure 8 Crystallization peak temperature T_p versus cooling rate for neat iPP and PP nanocomposites.

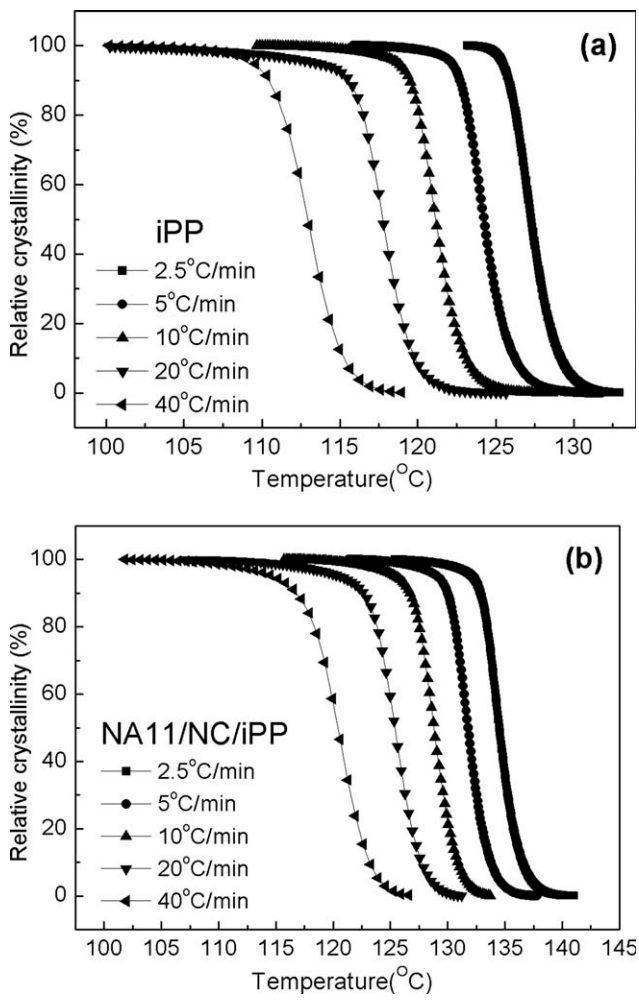

Figure 9 Relative crystallinity of (a) neat iPP and (b) NA11/NC/iPP at different cooling rates.

TABLE II
Nonisothermal Crystallization Kinetics Parameters for Pure iPP and PP Nanocomposites

Sample	Φ (°C/min)	T_p[a] (°C)	$t_{1/2}$ (s)	A	T_q[b] (°C)	n
iPP	2.5	127.0	150.7	−1.11	127.0	4.62 ± 0.22
	5	124.0	89.6	−0.99	123.8	
	10	120.9	44.0	−1.00	120.7	
	20	117.8	22.7	−0.96	117.3	
	40	113.0	10.0	−0.94	112.6	
NC/iPP	2.5	127.3	180.2	−1.00	127.1	4.35 ± 0.10
	5	124.3	83.6	−1.00	124.2	
	10	121.2	41.9	−0.99	121.0	
	20	117.9	25.0	−0.93	117.7	
	40	113.7	12.3	−0.89	113.0	
NA11/iPP	2.5	135.4	144.2	−1.15	135.2	4.31 ± 0.11
	5	132.6	76.1	−1.15	132.4	
	10	129.9	33.8	−1.17	129.6	
	20	127.0	21.3	−1.09	126.4	
	40	122.4	8.9	−0.96	122.0	
NA11/NC/iPP	2.5	134.3	155.3	−1.05	134.2	3.95 ± 0.13
	5	131.6	69.7	−1.09	131.5	
	10	128.7	29.3	−1.10	128.6	
	20	125.3	17.5	−0.97	125.1	
	40	120.6	9.2	−0.83	120.1	
NA11/NC/PP-*g*-MA/iPP 4.	2.5	132.8	187.9	−1.09	132.6	3.68 ± 0.18
	5	130.0	65.0	−1.12	129.9	
	10	127.0	36.5	−1.04	126.9	
	20	123.7	16.4	−0.99	123.5	
	40	119.0	13.9	−0.79	118.6	

[a] Determined form Figure 7.
[b] Calculated form Caze method.

stage. The values of a and $-aT_q$ can be determined from the slope and intercept of each straight line, and the results are also listed in Table II. It is noted that the linearity for the curves in Figure 10(a) (iPP) is better than those in Figure 10(b) (NA11/NC/iPP), which could be attributed to the effect of NA and NC on the crystallization process of iPP.

Straight lines can be obtained from plots of T_q versus ln φ/a under different cooling rates (Fig. 11), and Avrami exponents of iPP and nucleated iPP can be determined from the slope of each straight line. The results are also listed in Table II.

For both neat iPP and PP nanocomposites, it is found that $t_{1/2}$ decreases as the cooling rate increases, which indicate that the rate of crystallization is strongly dependent on the cooling rate.[29] In addition, at a given cooling rate, the crystallization rate of NA11/iPP is higher than of neat iPP, which could be attributed to the strong heterogeneous nucleation of NA11. However, the addition of NC results in the decrease of crystallization rate of iPP, which may result from retardation of NC on the transfer ability of iPP segment.[25,26] In addition, it is found that the combined addition of NA11 and NC resulted to the decrease of $t_{1/2}$ even in the presence of PP-*g*-MA especially at higher cooling rates.

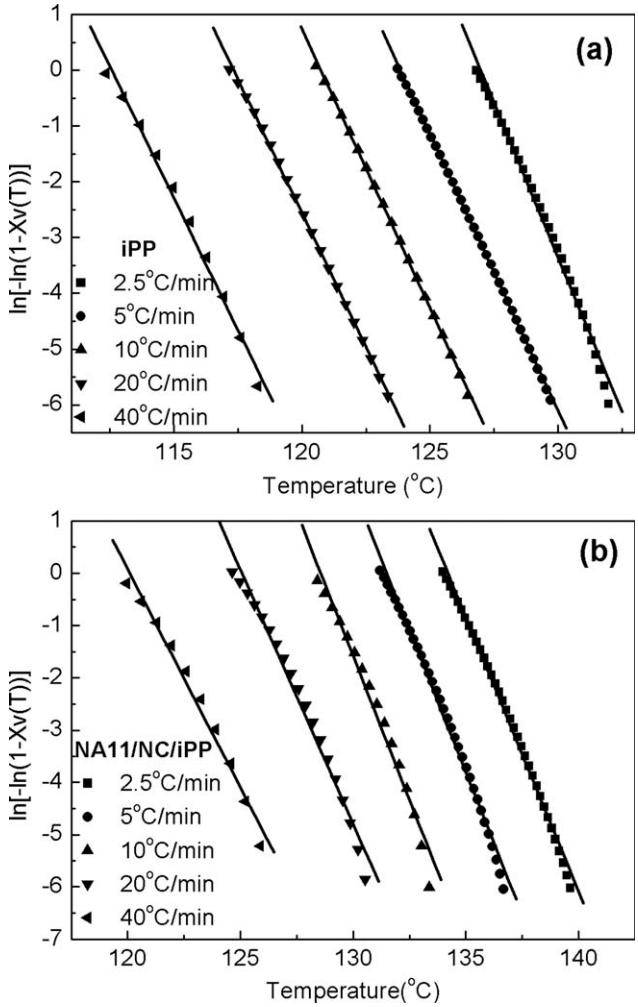

Figure 10 Plots of $\ln\{-\ln(1 - X_v(T))\}$ versus T for (a) neat iPP and (b) NA11/NC/iPP.

Comprehensively considering the effect of NA11 on the T_{cp} and $t_{1/2}$, it is concluded that the addition of NA11 into the nanocomposite could reduce cycle's time and raise the output of product.

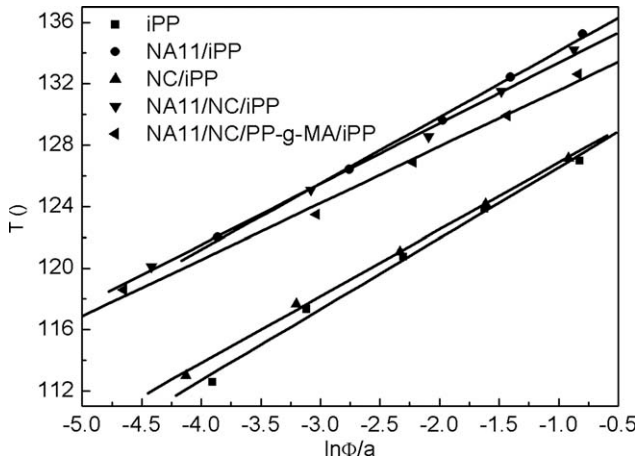

Figure 11 Plots of T_q versus ln ϕ/a for neat iPP and PP nanocomposites.

From Table II, the values of Avrami exponent (n) for PP nanocomposites decrease compared to neat iPP with the addition of NA11 and NC. The results indicated that their nuclei formation and spherulite growth were different and strongly affected by the presence of NA and nanoclay.

CONCLUSIONS

In this work, the α nucleating agent NA11 and nanoclay (I.44P) were used to investigate their combined effect on the mechanical properties and crystallization behavior of iPP. Meanwhile, the effect of the compatibilizer PP-*g*-MA on dispersion of NC was also studied. The main conclusions are summarized as follows:

The mechanical testing results indicated that the separate addition of NA11 and NC only increased the stiffness of iPP while the combined addition of NA11, NC, and PP-*g*-MA simultaneously improved stiffness and toughness of iPP. Compared to pure iPP, the tensile strength, the flexural modulus, and impact strength of iPP composites increased 9.7, 38.6, and 42.9%, respectively. The iPP composites showed better comprehensive mechanical properties comparing with separately adding NC or NA11 in iPP. The result indicated good synergistic effects of NC, NA11, and PP-*g*-MA in improving iPP mechanical properties.

WAXD patterns revealed NA11 and NC only induce α modification of iPP. SEM micrograph showed the PP-*g*-MA could effectively improve the dispersing of NC in iPP. The result is consistent with the effect of PP-*g*-MA on the mechanical properties of NC/iPP system. The NA NA11 could greatly decrease the crystals size of iPP while NC slightly affects it from the POM micrographs. The result is in agreement with the effect of NA11 and NC on the crystallization temperature of iPP.

The Caze method was applied to study the nonisothermal crystallization kinetics of pure iPP and PP nanocomposites. The result indicated that the addition of NC slightly increases crystallization temperature of iPP especially at higher cooling rates, while the NA NA11 greatly increases T_{cp} of NC nanocomposites. The addition of NA11 into the nanocomposite could significantly reduce cycle's time and raise the output of product. The addition of NAs overcomes the shortcoming of low crystallization rate of NC nanocomposites, which is the highlight of the compounded addition of NA and nanoclay in iPP. The values of Avrami exponent (n) of neat iPP and PP nanocomposites indicated that nuclei formation and spherulite growth of iPP were strongly affected by the presence of NA, nanoclay, and PP-*g*-MA.

References

1. Verga, J. In Polypropylene: Structure, Blends and Composites, Vol. 2; Chapman & Hall: London, 1995; p 56–58.
2. Balzano, L.; Rastogi, S.; Peters, G. W. M. Macromolecules 2008, 41, 399.
3. Liang, S.; Zhang, Y. Polym-Plast Technol Eng 2006, 45, 439.
4. Kristiansen, M.; Werner, M.; Tervoort, T.; Smith, P. Macromolecules 2003, 36, 5150.
5. Thierry, A.; Straupé, C.; Wittmann, J. C.; Lotz, B. Macromol Symp 2006, 241, 103.
6. Grein, C.; Plummer, C. J. G.; Kausch, H. H.; Germain, Y.; Beguelin, P. Polymer 2002, 43, 3279.
7. Chen, H. B.; Karger-Kocsis, J.; Wu, J. S.; Varga, J. Polymer 2002, 43, 6505.
8. Kotek, J.; Raab, M.; Baldrian, J.; Grellmann, W. J Appl Polym Sci 2002, 85, 1174.
9. Zhang, Y.; Xin, Z. J Appl Polym Sci 2006, 100, 4868.
10. Wu, J. Y.; Wu, T. M.; Chen, W. Y.; Tsai, S. J.; Kuo, W. F.; Chang, G. Y. J Polym Sci Polym Phys 2005, 43, 3242.
11. Tjong, S. C.; Bao, S. P.; Hang, G. D. J Polym Sci Polym Phys 2005, 43, 3112.
12. Mishra, S.; Sonawane, S. H.; Singh, R. P.; Bendale, A.; Patil, K. J Appl Polym Sci 2004, 94, 116.
13. Alexandre, M.; Dubois, P. Mater Sci Eng R 2000, 28, 1.
14. Giannelis, E. P. Adv Mater 1996, 8, 29.
15. Velasco, J. I.; Ardanuy, M.; Miralles, L.; Ortiz, S.; Maspoch, M. L.; Sánchez-Soto, M.; Santana, O. Macromol Symp 2005, 221, 63.
16. Velasco, J. I.; Ardanuy, M.; Realinho, V.; Antunes, M.; Fernandez, A. I.; Gonzalez-Pena, J. I.; Rodriguez-Perez, M. A.; de Saja, J. A. J Appl Polym Sci 2006, 102, 1213.
17. Kawasumi, M.; Hasegawa, N.; Kato, M.; Usuki, A.; Okada, A. Macromolecules 1997, 30, 6333.
18. Dal Castel, C.; Pelegrini, T.; Barbosa, R. V.; Liberman, S. A.; Mauler, R. S. Compos A-Appl Sci Manuf 2010, 41, 185.
19. Turner-Jones, A.; Aizlewood, J. M.; Beckett, D. R. Makromol Chem 1964, 75, 134.
20. Avrami, M. J Chem Phys 1939, 7, 1103.
21. Avrami, M. J Chem Phys 1940, 8, 212.
22. Ozawa, T. Polymer 1971, 12, 150.
23. Caze, C.; Devaux, E.; Crespy, A. Polymer 1997, 38, 497.
24. Kim, P. C.; Gan, S. N.; Chee, K. K. Polymer 1999, 40, 253.
25. Raka, L.; Bogoeva-Gaceva, G.; Loos, J. J Therm Anal Calorim 2010, 100, 629.
26. Pavlidou, S.; Papaspyrides, C. D. Prog Polym Sci 2008, 33, 1119.
27. Natta, G.; Corradini, P. Nuovo Cimento Suppl 1960, 15, 40.
28. Bassett, D. C.; Block, S.; Piermarini, G. J. J Appl Phys 1974, 45, 4146.
29. Zhao, S. C.; Cai, Z.; Xin, Z. Polymer 2008, 49, 2745.